INORGANIC CHEMISTRY FRONTIERS

RESEARCH ARTICLE

View Article Online
View Journal | View Issue

Cite this: *Inorg. Chem. Front.*, 2023, **10**, 1431

High-efficiency electrosynthesis of ammonia with selective reduction of nitrite over an Ag nanoparticle-decorated TiO_2 nanoribbon array†

Xiaoya Fan,[a,b] Xun He,[b] Xianchang Ji,[b] Longcheng Zhang,[b] Jun Li,[b] Long Hu,[b] Xiuhong Li,[b] Shengjun Sun,[c] Dongdong Zheng,[b] Yongsong Luo,[b] Yan Wang,[b] Lisi Xie,[d] Qian Liu,[d] Binwu Ying *[a] and Xuping Sun *[b,c]

Received 14th November 2022,
Accepted 11th January 2023

DOI: 10.1039/d2qi02409h

rsc.li/frontiers-inorganic

Electrochemical nitrite (NO_2^-) reduction can yield value-added ammonia (NH_3) while removing NO_2^- as an environmental pollutant in wastewater; however, it involves a six-electron transfer process and requires highly efficient and selective electrocatalysts. In this study, we report high-efficiency electrosynthesis of NH_3 *via* NO_2^- reduction enabled by an Ag nanoparticle-decorated TiO_2 nanoribbon array on a titanium plate (Ag@TiO_2/TP). When tested in 0.1 M NaOH containing 0.1 M NO_2^-, such Ag@TiO_2/TP shows a large NH_3 yield of 514.3 μmol h^{-1} cm^{-2} and a high faradaic efficiency of 96.4% at −0.5 V *vs.* a reversible hydrogen electrode. Significantly, it also demonstrates excellent durability for 12 h electrolysis.

Ammonia (NH_3) is widely applied to manufacture nitrogen fertilizers, explosives, chemical products, *etc.*, and it is also considered as an attractive hydrogen carrier and zero-carbon fuel.[1–3] Although the Haber–Bosch method realizes industrial NH_3 synthesis from hydrogen and nitrogen under high temperature and high pressure, this process is highly energy-intensive and emits a mass of greenhouse gases.[4] Electrochemical nitrogen reduction is thus deemed as a potential alternative to the Haber–Bosch process for ambient NH_3 synthesis, although the competitive hydrogen evolution reaction and unsatisfactory adsorption and cleavage effects of N_2 severely hinder the selectivity and activity of the electrochemical nitrogen reduction reaction.[5–14]

NH_3 synthesis *via* electrochemical nitrite (NO_2^-) reduction, in contrast, needs lower energy to cleave the N=O bond with faster reaction kinetics and achieves higher reaction substrate concentrations, leading to a larger NH_3 yield and higher faradaic efficiency (FE).[1,15,16] In addition, excess NO_2^- accumulated in groundwater could destroy the ecological balance and harm human health.[17] Electrochemical conversion of waste NO_2^- can produce value-added NH_3 under ambient conditions and simultaneously remove NO_2^-, which provides a solution for restoring the imbalance in the global nitrogen cycle. However, the electrochemical NO_2^- reduction reaction (NO_2^-RR) involves a complex six-electron pathway with various possible by-products (N_2H_4, N_2, and H_2), thus requiring highly active catalysts for selective NO_2^--to-NH_3 conversion.[18–27]

Noble metal (Au,[28] Pd,[28,29] Ru,[30] Ir,[31] Pt[32])-based catalysts are active for the NO_2^-RR, but their scarcity hinders large-scale applications. Compared with the above noble metals, Ag is relatively low in price and high in abundance, and it also performs efficiently in NO_2^- reduction electrocatalysis.[33] As an Earth-abundant transition metal oxide with high chemical and structural stability, TiO_2 is widely used as a support to load noble metal nanoparticles for catalysis applications.[34–39] Our recent studies also suggest that it is active for the NO_2^-RR and its activity can be enhanced by introducing oxygen vacancies[40] and P doping.[41] We believe that TiO_2 could be an ideal support for Ag nanoparticles for an enhanced NO_2^--to-NH_3 conversion performance with much less usage of noble metals, which, however, has not been reported to date.

In this study, we constructed an Ag nanoparticle-decorated TiO_2 nanoribbon array on a titanium plate (Ag@TiO_2/TP) as a highly selective NO_2^-RR catalyst for NH_3 synthesis. When tested in NO_2^--containing solution, Ag@TiO_2/TP is capable of delivering a large NH_3 yield of 514.3 μmol h^{-1} cm^{-2} with a high FE of 96.4% at −0.5 V *vs.* a reversible hydrogen electrode (RHE). Furthermore, Ag@TiO_2/TP exhibits robust stability for long-term electrolysis.

As shown in Fig. 1a, Ag@TiO_2/TP was synthesized through a hydrothermal method in an alkaline solution, Ag^+ exchange,

[a]*Department of Laboratory Medicine, West China Hospital, Sichuan University, Chengdu 610041, Sichuan, China. E-mail: yingbinwu@scu.edu.cn*
[b]*Institute of Fundamental and Frontier Sciences, University of Electronic Science and Technology of China, Chengdu 610054, Sichuan, China. E-mail: xpsun@uestc.edu.cn , xpsun@sdnu.edu.cn*
[c]*College of Chemistry, Chemical Engineering and Materials Science, Shandong Normal University, Jinan 250014, Shandong, China*
[d]*Institute for Advanced Study, Chengdu University, Chengdu 610068, Sichuan, China*
†Electronic supplementary information (ESI) available: Experimental section and supplementary figures. See DOI: https://doi.org/10.1039/d2qi02409h

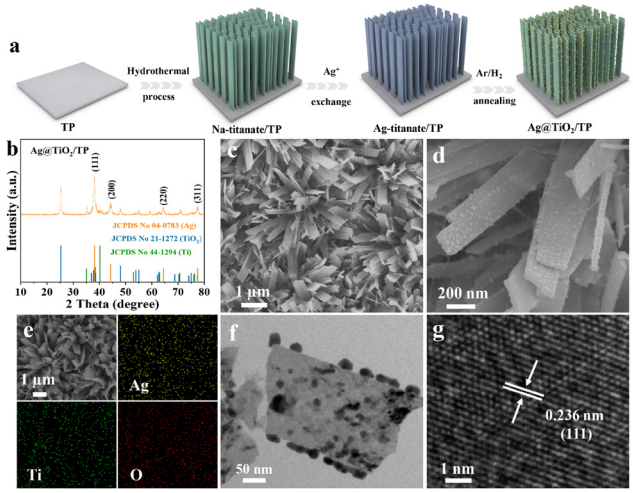

Fig. 1 (a) Schematic illustration of the fabrication process of $Ag@TiO_2$/TP. (b) XRD pattern and (c) and (d) SEM images of $Ag@TiO_2$/TP. (e) SEM and corresponding elemental mapping images of $Ag@TiO_2$/TP. (f) TEM and (g) HRTEM images of $Ag@TiO_2$.

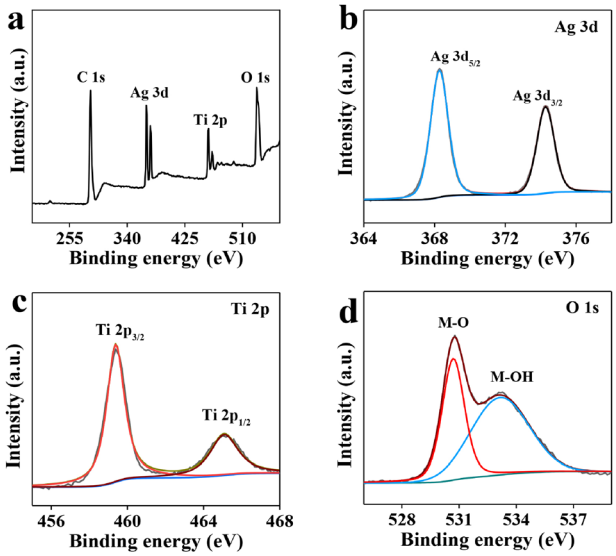

Fig. 2 (a) XPS survey spectrum, and high resolution XPS spectra in the (b) Ag 3d, (c) Ti 2p, and (d) O 1s regions of $Ag@TiO_2$.

and an annealing process under an Ar/H_2 atmosphere (see the ESI† for details). Fig. 1b depicts the X-ray diffraction (XRD) pattern of $Ag@TiO_2$/TP. The diffraction peaks at 38.15°, 44.30°, 64.43°, and 77.50° correspond to the (111), (200), (220), and (311) lattice planes of Ag, respectively (JCPDS No. 04-0783),[33] while the other diffraction peaks can be assigned to metallic Ti (JCPDS No. 44-1294) and TiO_2 (JCPDS No. 21-1272), and these are in accordance with those for TiO_2/TP (Fig. S1†). As depicted in Fig. S2 and S3,† the scanning electron microscopy (SEM) images show that the TiO_2 nanoribbon array was grown on TP. With regard to $Ag@TiO_2$/TP, plenty of nanoparticles are decorated on the surface of the TiO_2 nanoribbon (Fig. 1c and d). Additionally, the SEM image and corresponding energy-dispersive X-ray (EDX) elemental mapping images of $Ag@TiO_2$/TP confirm the existence of Ag, Ti, and O elements with a homogeneous distribution (Fig. 1e). Furthermore, the result of the EDX spectrum confirms that the Ag content in $Ag@TiO_2$/TP is approximately 13.63% (Fig. S4†). The transmission electron microscopy (TEM) image also provides evidence of the formation of a large number of nanoparticles without agglomeration on the nanoribbon, as shown in Fig. 1f. A high-resolution TEM (HRTEM) image taken from one such nanoparticle displays a lattice spacing of 0.236 nm indexed to the (111) plane of Ag (Fig. 1g). All these observations confirm the successful fabrication of an Ag nanoparticle-decorated TiO_2 nanoribbon array.

The X-ray photoelectron spectroscopy (XPS) survey spectrum (Fig. 2a) also shows the presence of Ag, O, and Ti elements. The Ag 3d region spectrum (Fig. 2b) is divided into two peaks at 368.28 and 374.28 eV, which are ascribed to Ag $3d_{5/2}$ and Ag $3d_{3/2}$, respectively.[42,43] In the Ti 2p spectrum, two fitting peaks at 459.38 and 465.08 eV are assigned to Ti $2p_{3/2}$ and Ti $2p_{1/2}$, respectively (Fig. 2c).[44,45] In addition, two fitting peaks in the O 1s spectrum are attributed to metal–oxygen bonds (M–O, 530.78 eV) and adsorbed surface hydroxyl groups (M–OH, 533.18 eV) (Fig. 2d).[42,45]

The electrochemical experiments of $Ag@TiO_2$/TP, Ag/TP, and TiO_2/TP toward the NO_2^-RR were implemented in Ar-saturated NO_2^--free and NO_2^--containing 0.1 M NaOH electrolytes. UV–vis spectra and related calibration curves are depicted in Fig. S5 and S6.† Linear scanning voltammetry (LSV) of $Ag@TiO_2$/TP was firstly conducted. Obviously, a markedly enhanced current density (j) emerges upon the addition of NO_2^- (Fig. 3a), verifying that $Ag@TiO_2$/TP enables efficient NO_2^- reduction. In comparison, Ag/TP and TiO_2/TP display lower j with NO_2^--containing electrolytes (Fig. S7†), confirming that the electrocatalytic NO_2^-RR activity of $Ag@TiO_2$/TP is superior to those of Ag/TP

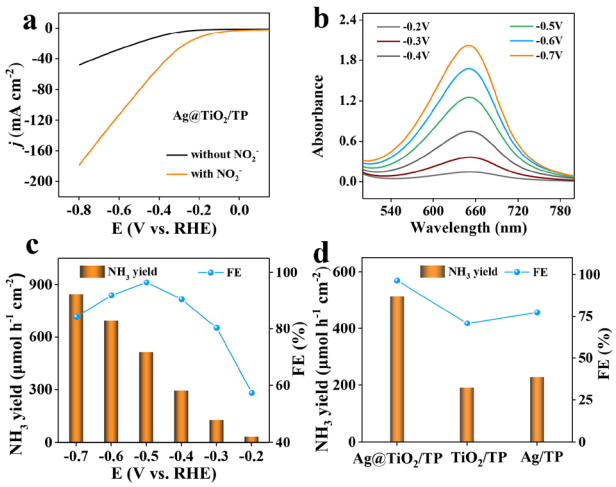

Fig. 3 (a) LSV curves of $Ag@TiO_2$/TP in 0.1 M NaOH with/without 0.1 M NO_2^-. (b) UV–vis spectra of $Ag@TiO_2$/TP at various potentials. (c) NH_3 yields and FEs of $Ag@TiO_2$/TP at various potentials. (d) Comparison of NH_3 yields and FEs of $Ag@TiO_2$/TP, TiO_2/TP, and Ag/TP at −0.5 V.

and TiO_2/TP. Chronoamperometry (CA) measurements at given potentials (from −0.2 V to −0.7 V) were then executed to study the NH_3-generation ability of Ag@TiO_2/TP (Fig. S8†), where the peak intensity of the relevant UV–vis spectra strengthens with an increase in the given potential (Fig. 3b), manifesting that a more negative potential results in more NH_3. Furthermore, we evaluated NH_3 FEs and yields of Ag@TiO_2/TP in test windows (Fig. 3c). Noticeably, as the cathode potential negatively shifts, the NH_3 yields of Ag@TiO_2/TP progressively increase, and eventually the largest value of 846.3 μmol h^{-1} cm^{-2} (14 387.1 μg h^{-1} cm^{-2}) at −0.7 V is obtained. Furthermore, the maximum FE of NH_3 production is 96.4% at −0.5 V with an NH_3 yield of 514.3 μmol h^{-1} cm^{-2} (8743.1 μg h^{-1} cm^{-2}), confirming an excellent NO_2^-RR electrocatalyst. The NH_3 yields and FEs of Ag@TiO_2/TP exceed those of most reported NO_2^-RR electrocatalysts (Table S1†). As shown in Fig. 3d, Ag@TiO_2/TP exhibits a much better performance than Ag/TP (77.38%, 228.5 μmol h^{-1} cm^{-2}) and TiO_2/TP (70.8%, 190.9 μmol h^{-1} cm^{-2}).

The NO_2^- reduction process of Ag@TiO_2/TP was further assessed by quantifying various by-products (N_2H_4, H_2, and N_2). As exhibited in Fig. S9,† no N_2H_4 signals were monitored as was proved by identical UV–vis absorption spectral peaks at different potentials. Meanwhile, traces of H_2 and N_2 were detected (Fig. 4a) with the maximal H_2 and N_2 yields being 2.82 μmol h^{-1} cm^{-2} and 1.85 μmol h^{-1} cm^{-2}, with FEs of 4.9% and 1.42%, respectively, much lower than that of NH_3 at every potential, verifying the superb selectivity of such Ag@TiO_2/TP electrocatalysts for NH_3 synthesis. Furthermore, the partial current densities ($j_{partial}$) of Ag@TiO_2/TP for NH_3 reach −122.1 mA cm^{-2} at −0.7 V, clearly higher than that of H_2 (−4.1 mA cm^{-2}) and N_2 (−1.04 mA cm^{-2}) (Fig. 4b), again proving great NO_2^-RR selectivity towards NH_3 electrosynthesis. Control experiments were then performed to determine whether the synthesized NH_3 just comes from the NO_2^-RR on Ag@TiO_2/TP. It is clearly seen that the amounts of NH_3 generated after 1 h of electrolysis in a blank solution (0.29 μg) and open circuit potential (OCP, 0.66 μg) are extremely small (Fig. S10†), which excludes possible interference factors from the electrolytic solution and device.

Six alternative-cycle measurements were then carried out in NO_2^--free/NO_2^--containing electrolytes at −0.5 V, and NH_3 only is generated in NO_2^--containing electrolytes (Fig. 4c), demonstrating that NH_3 just originates from NO_2^- *via* the NO_2^-RR on Ag@TiO_2/TP. Additionally, stability is an extremely important parameter of the NO_2^-RR process for NH_3 synthesis. We thus implemented a 12 h electrolysis test, as displayed in Fig. 4d, and the Ag@TiO_2/TP electrode maintained an initial j of nearly 100% with almost no fluctuation, confirming the excellent tolerance of our catalyst. Furthermore, we carried out 8 consecutive measurements on Ag@TiO_2/TP at −0.5 V, and the volatility of NH_3 yields and FEs was negligible, again proving the durability of Ag@TiO_2/TP (Fig. 4e and S11†), which is also in good accordance with the LSV curve (Fig. S12†), XRD pattern (Fig. S13†), and SEM images (Fig. S14†) of Ag@TiO_2/TP after long-term electrolysis. These results suggest that Ag@TiO_2/TP has excellent stability for the electrocatalytic reduction of NO_2^- to NH_3.

In summary, a Ag nanoparticle-decorated TiO_2 nanoribbon array is proved to be an efficient and stable NO_2^-RR catalyst for NO_2^--to-NH_3 conversion in an alkaline electrolyte, producing a remarkable NH_3 yield of 8743.1 μg h^{-1} cm^{-2} with a large FE of 96.4%. This study not only offers a highly selective electrocatalyst for ambient NH_3 synthesis *via* NO_2^- reduction, but also opens up a new avenue to construct a nanostructured Ag/TiO_2 hybrid array for applications.

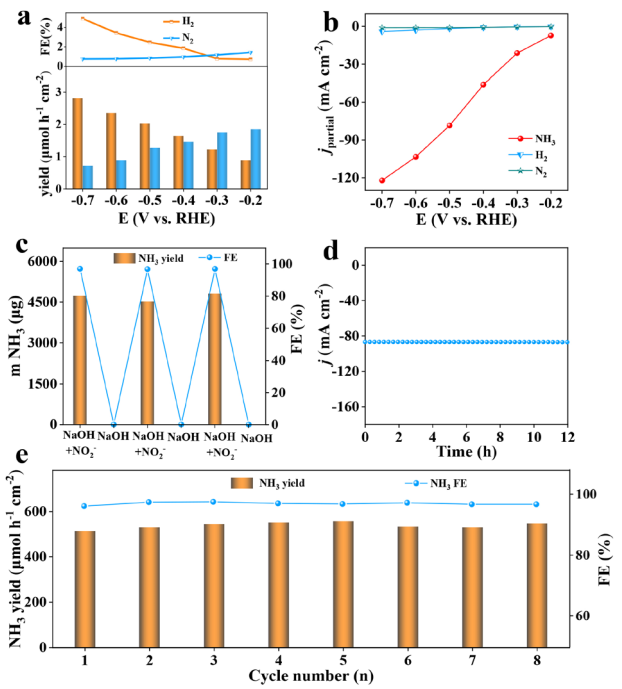

Fig. 4 (a) Yields and FEs of N_2 and H_2 of Ag@TiO_2/TP at different potentials. (b) $j_{partial}$ of NH_3, N_2, and H_2 of Ag@TiO_2/TP at different potentials. (c) NH_3 yields and FEs of Ag@TiO_2/TP during the alternating cycling tests. (d) Time-dependent current density curve during 12 h electrolysis of Ag@TiO_2/TP at −0.5 V. (e) Recycling tests of Ag@TiO_2/TP at −0.5 V.

Conflicts of interest

There are no conflicts to declare.

Acknowledgements

This work was supported by the National Natural Science Foundation of China (No. 22072015).

References

1 J. Liang, Q. Liu, A. A. Alshehri and X. Sun, Recent advances in nanostructured heterogeneous catalysts for N-cycle electrocatalysis, *Nano Res. Energy*, 2022, **1**, e9120010.

2 J. Liang, W. Hu, B. Song, T. Mou, L. Zhang, Y. Luo, Q. Liu, A. A. Alshehri, M. S. Hamdy, L. Yang and X. Sun, Efficient nitric oxide electroreduction toward ambient ammonia synthesis catalyzed by a CoP nanoarray, *Inorg. Chem. Front.*, 2022, **9**, 1366–1372.
3 D. Qi, F. Lv, T. Wei, M. Jin, G. Meng, S. Zhang, Q. Liu, W. Liu, D. Ma, M. S. Hamdy, J. Luo and X. Liu, High-efficiency electrocatalytic NO reduction to NH_3 by nanoporous VN, *Nano Res. Energy*, 2022, **1**, e9120022.
4 I. Dybkjaer, in *Ammonia, catalysis and manufacture*, ed. A. Nielsen, Springer, Heidelberg, 1995, pp. 199–327.
5 Y. Ji, L. Li, W. Cheng, Y. Xiao, C. Li and X. Liu, A CeP nanoparticle-reduced graphene oxide hybrid: an efficient electrocatalyst for the NH_3 synthesis under ambient conditions, *Inorg. Chem. Front.*, 2021, **8**, 2103–2106.
6 L. Li, C. Tang, H. Jin, K. Davey and S.-Z. Qiao, Main-group elements boost electrochemical nitrogen fixation, *Chem*, 2021, **7**, 3232–3255.
7 N. Cao, Z. Chen, K. Zang, J. Xu, J. Zhong, J. Luo, X. Xu and G. Zheng, Doping strain induced Bi-Ti^{3+} pairs for efficient N_2 activation and electrocatalytic fixation, *Nat. Commun.*, 2019, **10**, 2877.
8 C. Guo, J. Ran, A. Vasileff and S. Qiao, Rational design of electrocatalysts and photo(electro)catalysts for nitrogen reduction to ammonia (NH_3) under ambient conditions, *Energy Environ. Sci.*, 2018, **11**, 45–56.
9 D. Chanda, R. Xing, T. Xu, Q. Liu, Y. Luo, S. Liu, R. A. Tufa, T. H. Dolla, T. Montini and X. Sun, Electrochemical nitrogen reduction: recent progress and prospects, *Chem. Commun.*, 2021, **57**, 7335–7349.
10 Y. Luo, Q. Li, Y. Tian, Y. Liu and K. Chu, Amorphization engineered VSe_{2-x} nanosheets with abundant Se-vacancies for enhanced N_2 electroreduction, *J. Mater. Chem. A*, 2022, **10**, 1742–1749.
11 Y. Li, Y. Liu, J. Wang, Y. Guo and K. Chu, Plasma-engineered NiO nanosheets with enriched oxygen vacancies for enhanced electrocatalytic nitrogen fixation, *Inorg. Chem. Front.*, 2020, **7**, 455–463.
12 S. Zhang, C. Zhao, Y. Liu, W. Li, J. Wang, G. Wang, Y. Zhang, H. Zhang and H. Zhao, Cu doping in CeO_2 to form multiple oxygen vacancies for dramatically enhanced ambient N_2 reduction performance, *Chem. Commun.*, 2019, **55**, 2952–2955.
13 C. Liu, S. Li, Z. Li, L. Zhang, H. Chen, D. Zhao, S. Sun, Y. Luo, A. A. Alshehri, M. S. Hamdy, Q. Liu and X. Sun, Ambient N_2-to-NH_3 fixation over CeO_2 nanoparticles decorated three-dimensional carbon skeleton, *Sustainable Energy Fuels*, 2022, **6**, 3344–3348.
14 Q. Li, P. Shen, Y. Tian, X. Li and K. Chu, Metal-free BN quantum dots/graphitic C_3N_4 heterostructure for nitrogen reduction reaction, *J. Colloid Interface Sci.*, 2022, **606**, 204–212.
15 X. He, X. Li, X. Fan, J. Li, D. Zhao, L. Zhang, S. Sun, Y. Luo, D. Zheng, L. Xie, A. M. Asiri, Q. Liu and X. Sun, Ambient electroreduction of nitrite to ammonia over Ni nanoparticle supported on molasses-derived carbon sheets, *ACS Appl. Nano Mater.*, 2022, **5**, 14246–14250.
16 S. Li, J. Liang, P. Wei, Q. Liu, L. Xie, Y. Luo and X. Sun, ITO@TiO_2 nanoarray: an efficient and robust NO_2^- reduction reaction electrocatalyst toward NH_3 production under ambient conditions, *eScience*, 2022, **2**, 382–388.
17 X. Zhu, X. Zeng, X. Chen, W. Wu and Y. Wang, Inhibitory effect of nitrate/nitrite on the microbial reductive dissolution of arsenic and iron from soils into pore water, *Ecotoxicology*, 2019, **28**, 528–538.
18 Q. Liu, Q. Liu, X. Lisi, L. Yue, T. Li, Y. Luo, N. Li, B. Tang, L. Yu and X. Sun, 3D FeOOH nanotube array: an efficient catalyst for ammonia electrosynthesis by nitrite reduction, *Chem. Commun.*, 2022, **58**, 5160–5163.
19 C. Wang, W. Zhou, Z. Sun, Y. Wang, B. Zhang and Y. Yu, Integrated selective nitrite reduction to ammonia with tetrahydroisoquinoline semi-dehydrogenation over a vacancy-rich Ni bifunctional electrode, *J. Mater. Chem. A*, 2021, **9**, 239–243.
20 L. Hu, D. Zhao, C. Liu, Y. Liang, D. Zheng, S. Sun, Q. Li, Q. Liu, Y. Luo, Y. Liao, L. Xie and X. Sun, Amorphous CoB nanoarray as a high-efficiency electrocatalyst for nitrite reduction to ammonia, *Inorg. Chem. Front.*, 2022, **9**, 6075–6079.
21 X. Zhang, Y. Wang, Y. Wang, Y. Guo, X. Xie, Y. Yu and B. Zhang, Recent advances in electrocatalytic nitrite reduction, *Chem. Commun.*, 2022, **58**, 2777–2787.
22 L. Ouyang, L. Yue, Q. Liu, Q. Liu, Z. Li, S. Sun, Y. Luo, A. A. Alshehri, M. S. Hamdy, Q. Kong and X. Sun, Cu nanoparticles decorated juncus-derived carbon for efficient electrocatalytic nitrite-to-ammonia conversion, *J. Colloid Interface Sci.*, 2022, **624**, 394–399.
23 J. Wang, T. Feng, J. Chen, V. Ramalingam, Z. Li, D. M. Kabtamu, J. He and X. Fang, Electrocatalytic nitrate/nitrite reduction to ammonia synthesis using metal nanocatalysts and bio-inspired metalloenzymes, *Nano Energy*, 2021, **86**, 106088.
24 L. Mattarozzi, S. Cattarina, N. Comissoa, P. Guerriero, M. Musiani, L. Vázquez-Gómez and E. Verlatoa, Electrochemical reduction of nitrate and nitrite in alkaline media at CuNi alloy electrodes, *Electrochim. Acta*, 2013, **89**, 488–496.
25 R. Zhang, S. Zhang, Y. Guo, C. Li, J. Liu, Z. Huang, Y. Zhao, Y. Li and C. Zhi, A Zn–nitrite battery as an energy-output electrocatalytic system for high-efficiency ammonia synthesis using carbon-doped cobalt oxide nanotubes, *Energy Environ. Sci.*, 2022, **15**, 3024–3032.
26 S. E. Braley, J. Xie, Y. Losovyj and J. M. Smith, Graphite conjugation of a macrocyclic cobalt complex enhances nitrite electroreduction to ammonia, *J. Am. Chem. Soc.*, 2021, **143**, 7203–7208.
27 Z. Chen, A. Jaworski, J. Chen, T. M. Budnyak, I. Szewczyk, A. Rokicińska, R. Dronskowski, N. Hedin, P. Kuśtrowski and A. Slabon, Graphitic nitrogen in carbon catalysts is important for the reduction of nitrite as revealed by naturally abundant ^{15}N NMR spectroscopy, *Dalton Trans.*, 2021, **50**, 6857–6866.

28 H. Li, S. Guo, K. Shin, M. S. Wong and G. Henkelman, Design of a Pd–Au nitrite reduction catalyst by identifying and optimizing active ensembles, *ACS Catal.*, 2019, **9**, 7957–7966.

29 H. Shin, S. Jung, S. Bae, W. Lee and H. Kim, Nitrite reduction mechanism on a Pd surface, *Environ. Sci. Technol.*, 2014, **48**, 12768–12774.

30 X. Huo, D. J. Van Hoomissen, J. Liu, S. Vyas and T. J. Strathmann, Hydrogenation of aqueous nitrate and nitrite with ruthenium catalysts, *Appl. Catal., B*, 2017, **211**, 188–198.

31 H. Li, C. Yan, H. Guo, K. Shin, S. M. Humphrey, C. J. Werth and G. Henkelman, Cu_xIr_{1-x} nanoalloy catalysts achieve near 100% selectivity for aqueous nitrite reduction to NH_3, *ACS Catal.*, 2020, **10**, 7915–7921.

32 M. C. Figueiredo, V. Climent and J. M. Feliu, Nitrite reduction on bismuth modified Pt (111) surfaces in different electrolytic media, *Electrocatalysis*, 2011, **2**, 255–262.

33 Q. Liu, G. Wen, D. Zhao, L. Xie, S. Sun, L. Zhang, Y. Luo, A. A. Alshehri, M. S. Hamdy, Q. Kong and X. Sun, Nitrite reduction over Ag nanoarray electrocatalyst for ammonia synthesis, *J. Colloid Interface Sci.*, 2022, **623**, 513–519.

34 S. Chang and X. Xu, Au nanocrystals decorated TiO_2 nanotubes for photocatalytic nitrogen fixation into ammonia, *Inorg. Chem. Front.*, 2020, **7**, 620–624.

35 W. Shi, A.-H. Park, S. Xu, P. J. Yoo and Y.-U. Kwon, Continuous and conformal thin TiO_2-coating on carbon support makes Pd nanoparticles highly efficient and durable electrocatalyst, *Appl. Catal., B*, 2021, **284**, 119715.

36 A. Shoaib, M. Ji, H. Qian, J. Liu, M. Xu and J. Zhang, Noble metal nanoclusters and their in situ calcination to nanocrystals: precise control of their size and interface with TiO_2 nanosheets and their versatile catalysis applications, *Nano Res.*, 2016, **9**, 1763–1774.

37 S. Zhang, W. Wang, Y. Gao, S. Deng, L. Ding, H. Zhuo, Z. Bao, W. Ji, C. Qiu and J. Wang, Pd-Co alloy supported on TiO_2 with oxygen vacancies for efficient N_2 and O_2 electrocatalytic reduction, *Appl. Surf. Sci.*, 2021, **567**, 150680.

38 L.-N. Chen, S.-H. Wang, P.-Y. Zhang, Z.-X. Chen, L. Xiao, H.-J. Yang, T. Sheng, W.-F. Lin, N. Tian, S.-G. Sun and Z.-Y. Zhou, Ru nanoparticles supported on partially reduced TiO_2 as highly efficient catalyst for hydrogen evolution, *Nano Energy*, 2021, **88**, 106211.

39 Z.-W. Wei, H.-J. Wang, C. Zhang, K. Xu, X.-L. Lu and T.-B. Lu, Reversed charge transfer and enhanced hydrogen spillover in platinum nanoclusters anchored on titanium oxide with rich oxygen vacancies boost hydrogen evolution reaction, *Angew. Chem., Int. Ed.*, 2021, **60**, 16622–16627.

40 D. Zhao, J. Liang, J. Li, L. Zhang, K. Dong, L. Yue, Y. Luo, Y. Ren, Q. Liu, M. S. Hamdy, Q. Kong, Q. Liu and X. Sun, A TiO_{2-x} nanobelt array with oxygen vacancies: an efficient electrocatalyst toward nitrite conversion to ammonia, *Chem. Commun.*, 2022, **58**, 3669–3672.

41 L. Ouyang, X. He, S. Sun, Y. Luo, D. Zheng, J. Chen, Y. Li, Y. Lin, Q. Liu, A. M. Asirif and X. Sun, Enhanced electrocatalytic nitrite reduction to ammonia over P-doped TiO_2 nanobelt array, *J. Mater. Chem. A*, 2022, **10**, 23494–23498.

42 Q. Qin, Y. Li, W. Bu, L. Meng, X. Chuai, Z. Zhou and C. Hu, Self-template-derived $ZnCo_2O_4$ porous microspheres decorated by Ag nanoparticles and their selective detection of formaldehyde, *Inorg. Chem. Front.*, 2021, **8**, 811–820.

43 Y. Fang, S. Zhang, Z.-P. Wu, D. Luan and X. W. Lou, A highly stable lithium metal anode enabled by Ag nanoparticle-embedded nitrogen-doped carbon macroporous fibers, *Sci. Adv.*, 2021, **7**, eabg3626.

44 Y. Guo, R. Zhang, S. Zhang, Y. Zhao, Q. Yang, Z. Huang, B. Dong and C. Zhi, Pd doping-weakened intermediate adsorption to promote electrocatalytic nitrate reduction on TiO_2 nanoarrays for ammonia production and energy supply with zinc-nitrate batteries, *Energy Environ. Sci.*, 2021, **14**, 3938–3944.

45 X. Fan, C. Ma, D. Zhao, Z. Deng, L. Zhang, Y. Wang, Y. Luo, D. Zheng, T. Li, J. Zhang, S. Sun, Q. Liu and X. Sun, Unveiling selective nitrate reduction to ammonia with Co_3O_4 nanosheets/TiO_2 nanobelt heterostructure catalyst, *J. Colloid Interface Sci.*, 2023, **630**, 714–720.